JACS
JOURNAL OF THE AMERICAN CHEMICAL SOCIETY
Article
Cite This: J. Am. Chem. Soc. 2018, 140, 11735−11744
pubs.acs.org/JACS

Effects of Polymer Coatings on Electrodeposited Lithium Metal

Jeffrey Lopez,[†,#] Allen Pei,[‡,#] Jin Young Oh,[†,∥] Ging-Ji Nathan Wang,[§] Yi Cui,[*,‡,⊥] and Zhenan Bao[*,†]

[†]Department of Chemical Engineering, [‡]Department of Materials Science and Engineering, and [§]Department of Chemistry, Stanford University, Stanford, California 94305, United States

[∥]Department of Chemical Engineering, Kyung Hee University, Yongin 17104, Republic of Korea

[⊥]Stanford Institute for Materials and Energy Sciences, SLAC National Accelerator Laboratory, Menlo Park, California 94025, United States

Supporting Information

ABSTRACT: The electrodeposition of lithium metal is a key process in next-generation, high energy density storage devices. However, the high reactivity of the lithium metal causes short cycling lifetimes and dendrite growth that can pose a serious safety issue. Recently, a number of approaches have been pursued to stabilize the lithium metal−electrolyte interface, including soft polymeric coatings that have shown the ability to enable high-rate and high-capacity lithium metal cycling, but a clear understanding of how to design and modify these coatings has not yet been established. In this work, we studied the effects of several polymers with systematically varied chemical and mechanical properties as coatings on the lithium metal anode. By examining the early stages of lithium metal deposition, we determine that the morphology of the lithium particles is strongly influenced by the chemistry of the polymer coating. We have identified polymer dielectric constant and surface energy as two key descriptors of the lithium deposit size. Low surface energy polymers were found to promote larger deposits with smaller surface areas. This may be explained by a reduced interaction between the coating and the lithium surface and thus an increase in the interfacial energy. On the other hand, high dielectric constant polymers were found to increase the exchange current and gave larger lithium deposits due to the decreased overpotentials at a fixed current density. We also observed that the thickness of the polymer coating should be optimized for each individual polymer. Furthermore, polymer reactivity was found to strongly influence the Coulombic efficiency. Overall, this work offers new fundamental insights into lithium electrodeposition processes and provides direction for the design of new polymer coatings to better stabilize the lithium metal anode.

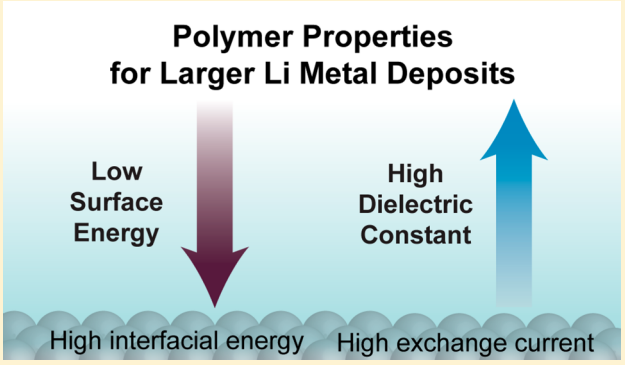

INTRODUCTION

Recently, research on stabilizing the lithium (Li) metal anode has received renewed attention because of Li's central importance to enable next-generation, high energy density electrochemical energy storage.[1,2] State-of-the-art lithium ion batteries (LIBs) are capable of achieving specific energies as high as 250 Wh kg^{-1}, but further improvement calls for the use of Li metal as the anode because of its increased capacity compared to that of graphite (3860 mAh g^{-1} vs 372 mAh g^{-1}) and low potential (−3.04 V vs the standard hydrogen electrode).[3] Additionally, high capacity Li-S and Li-O_2 battery chemistries depend on the use of Li metal anodes.[4−6] Although Li metal was heavily studied during the early stages of LIB research, focus moved away from the material due to safety issues and the commercial success of graphite anodes.[7] Recently, new experimental techniques and insights have allowed researchers to approach the problem again with fresh ideas and improved tools.[2,8−10] Even with this renewed effort, safety and cyclability challenges due to solid electrolyte interphase (SEI) formation and poor quality Li metal deposition remain.[1] In order to overcome these issues and effectively design solutions that improve the lifetime and safety of lithium metal batteries, a clear understanding of the surface reactivity and growth behavior of the lithium metal at the interface with the electrolyte is necessary.

The interface between the lithium metal anode and electrolyte, regardless liquid or solid, fundamentally controls how Li^+ ions are deposited on and stripped from the electrode. Approaches to stabilize this interface include the use of modified liquid electrolytes, solid electrolytes, and electrode coatings.[1,2,9−12] Highly concentrated electrolytes reduce the electrochemical decomposition of solvent molecules against the highly reactive Li metal surface,[13,14] and additives can enable smooth Li deposition by improving the ionic conductivity, mechanical properties, and chemical composition

Received: June 12, 2018
Published: August 28, 2018

DOI: 10.1021/jacs.8b06047
J. Am. Chem. Soc. 2018, 140, 11735−11744

of the SEI.[15−17] The most successful approaches that use solid electrolytes have focused on either high modulus polymer electrolytes to mechanically suppress the dendrites[18,19] or softer cross-linked polymer electrolytes that improve deposition through surface effects.[20−22] Engineered interfaces using thin carbon or boron nitride structures have also improved the deposition of Li metal.[23,24] Tailoring the Li metal interface with polymer coatings has been the focus of much recent study, and a variety of materials have been used including cross-linked films,[25] soft self-healing and adaptive coatings,[26−28] composites,[29] fluoropolymers,[30,31] and grafted coatings.[32] These polymer coatings have been shown to enable high-rate and high-capacity deposition. Using polymer coatings is attractive because of their ability to be easily processed and the potential for pairing with other electrolyte-based strategies. However, a clear understanding of how to design or modify these polymer coatings for a better control of the deposition and stripping of Li metal has yet to be developed.

Here we investigate the effects of polymer coatings on electrodeposited lithium by studying coatings with varied chemical and mechanical properties. We build upon previously reported theoretical studies of Li-polymer interfaces[33,34] in order to elucidate the important factors governing the interaction between these coatings and the Li metal deposits. We find that the local morphology is strongly influenced by the chemistry of the polymer and that both the Li/Li^+ exchange current and polymer surface energy influence this local Li morphology by modifying the energetics of the nucleation and growth processes. We also found that initial thickness of the polymer coating is an important parameter to optimize. In addition, we used microelectrodes to measure the exchange current for our polymer coatings and found that the dielectric constant of the polymer is correlated with the exchange current. This allows us to use two easily measurable bulk polymer properties (surface energy and dielectric constant) as descriptors for the effect of polymer coatings on the nucleation and growth of electrodeposited Li metal. Overall, this work provides new insights into lithium electrodeposition processes for future design and synthesis of new polymer coatings to better stabilize the Li metal anode.

RESULTS

Properties of Polymer Coatings. Recently, several approaches have been successful at improving Li metal deposition with polymer coatings.[25−32] However, there are still no well-defined guiding principles on polymer selection. In order to develop a clear fundamental picture of the processes affecting Li metal deposition, we prepared a number of polymer coatings with various chemical and mechanical properties to investigate the importance of these parameters to the quality of the electrodeposited Li metal. For this study, we systematically chose several different polymers that have been previously used in battery applications. Poly(ethylene oxide) (PEO) is a common solid polymer electrolyte, and polyurethane (PU) and poly(vinylidene fluoride) (PVDF) are common gel electrolytes. Additionally, PVDF and poly(vinylidene fluoride-*co*-hexafluoropropylene) (PVDF-HFP) are also common binder materials for composite electrodes. Poly(dimethylsiloxane) (PDMS) was tested because it has been used previously as a coating to stabilize Li metal.[25,27] We also modified the mechanical properties of our previously reported adaptive (self-healing) polymer (SHP) coating[26] with chemical cross-linking to obtain a self-healing elastomer (SHE) with different mechanical properties but almost identical chemistry (Figure S1). The thermal and mechanical properties of the polymers were characterized in detail (Table 1, Figures S2−S4), and the following distinct groupings can be observed (Figure 1). PEO, PVDF, and PVDF-HFP are rigid, semicrystalline solids exhibiting high initial modulus and plastic deformation after strain is applied. They are characterized by frequency-independent storage modulus and clear first-order phase transitions corresponding to the melting of the their crystalline domains. The stress−strain curves in Figure S2 show that these properties will give rise to tough but deformable polymer coatings at room temperature. The SHP and PDMS coatings are highly adaptable to mechanical strain due to the viscoelastic nature of these two polymers. Both polymers have liquid-like mechanical properties at low frequencies with the loss modulus dominating over the storage modulus (Figure S3). While the SHP is a flowable viscoelastic material, the SHE is a covalently cross-linked elastic solid. Similarly, the PU used here is a soft elastomer with high stretchability and low glass transition temperature (T_g). These elastic coatings should be able to deform and potentially recover from applied strain, but these films will not have the adaptive qualities of the SHP and PDMS due to solid-like properties of both elastomers. Even at long time scales, the SHE and PU both behave as solids and will not significantly flow or adapt without external stimuli. Overall, PEO, PVDF, and PVDF-HFP have the mechanical properties of traditional thermoplastics, PU and SHE are soft elastomers, and PDMS and SHP are viscoelastic materials.

Table 1. Thermal and Mechanical Properties of Polymers Used in This Study

polymer	E^a (MPa)	G'^b (MPa)	$T_g{}^c$ (°C)	$T_m{}^e$ (°C)
PEO	82.8	219	n.d.[d]	64
PU	1.4	0.51	n.d.	n.d.
PVDF	171	377	44	155
PVDF-HFP	335	489	55	159
SHP	0.11	variable	−13	n.d.
SHE	0.29	variable	−2	n.d.

[a]Young's modulus. [b]Plateau storage modulus. [c]Glass transition temperature. [d]Not detected. [e]Melting point.

The interaction of the polymers with the liquid electrolyte will also be an important factor in the battery environment, so the swelling of the polymers after 24 h in the electrolyte was measured (Table S1). PVDF, PVDF-HFP, and PDMS only swelled ∼30%, while the hydrophilic polymers swelled significantly more. PU swelled up to ∼600%, and the PEO formed a gel with the large excess of electrolyte used to measure the swelling. This amount of swelling should be considered an upper limit for the amount that the coatings may swell in the coin cells due to the limited electrolyte volume and significant pressure. The actual amount of swelling that occurs for the coatings is difficult to quantify. The moduli of the swollen coatings will certainly be lower than that of the bulk polymers, but measuring the swollen mechanical properties was beyond the scope of this study due to the lack of correlation between the mechanics of the coating and the ultimate Li morphology discussed below. Additionally, swelling was previously found to have a minimal effect on the viscoelastic properties of the SHP.[26] The varied mechanical and chemical properties of these coatings cover a broad range

DOI: 10.1021/jacs.8b06047
J. Am. Chem. Soc. 2018, 140, 11735−11744

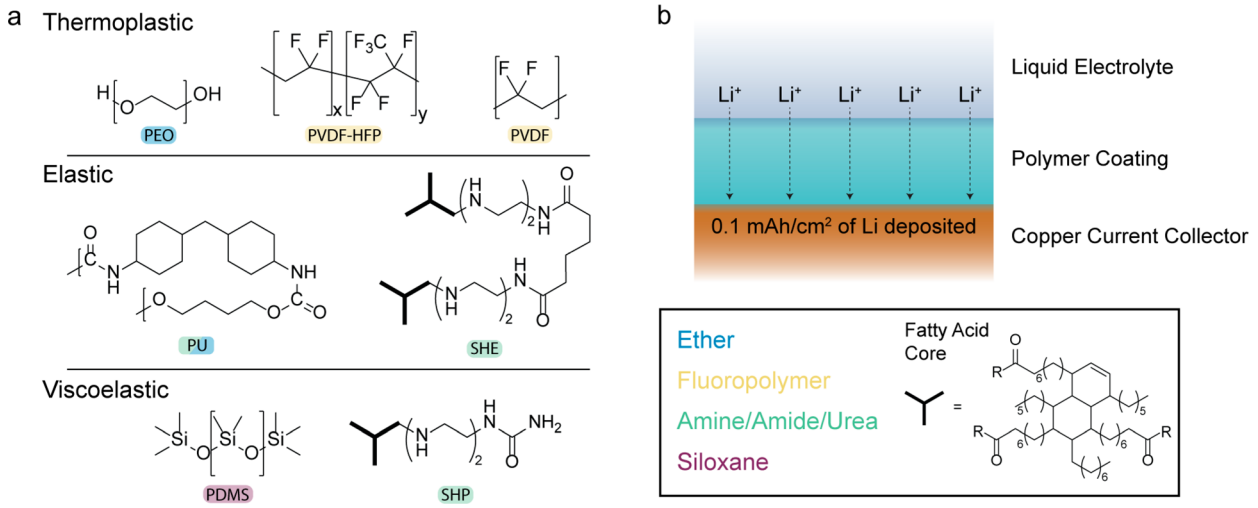

Figure 1. (a) Chemical structures of the polymer coatings used in this study. Coloring of the label corresponds to the chemical functionality of the polymer. (b) Diagram of the conditions used to study the initial stages of Li metal growth under polymer coatings.

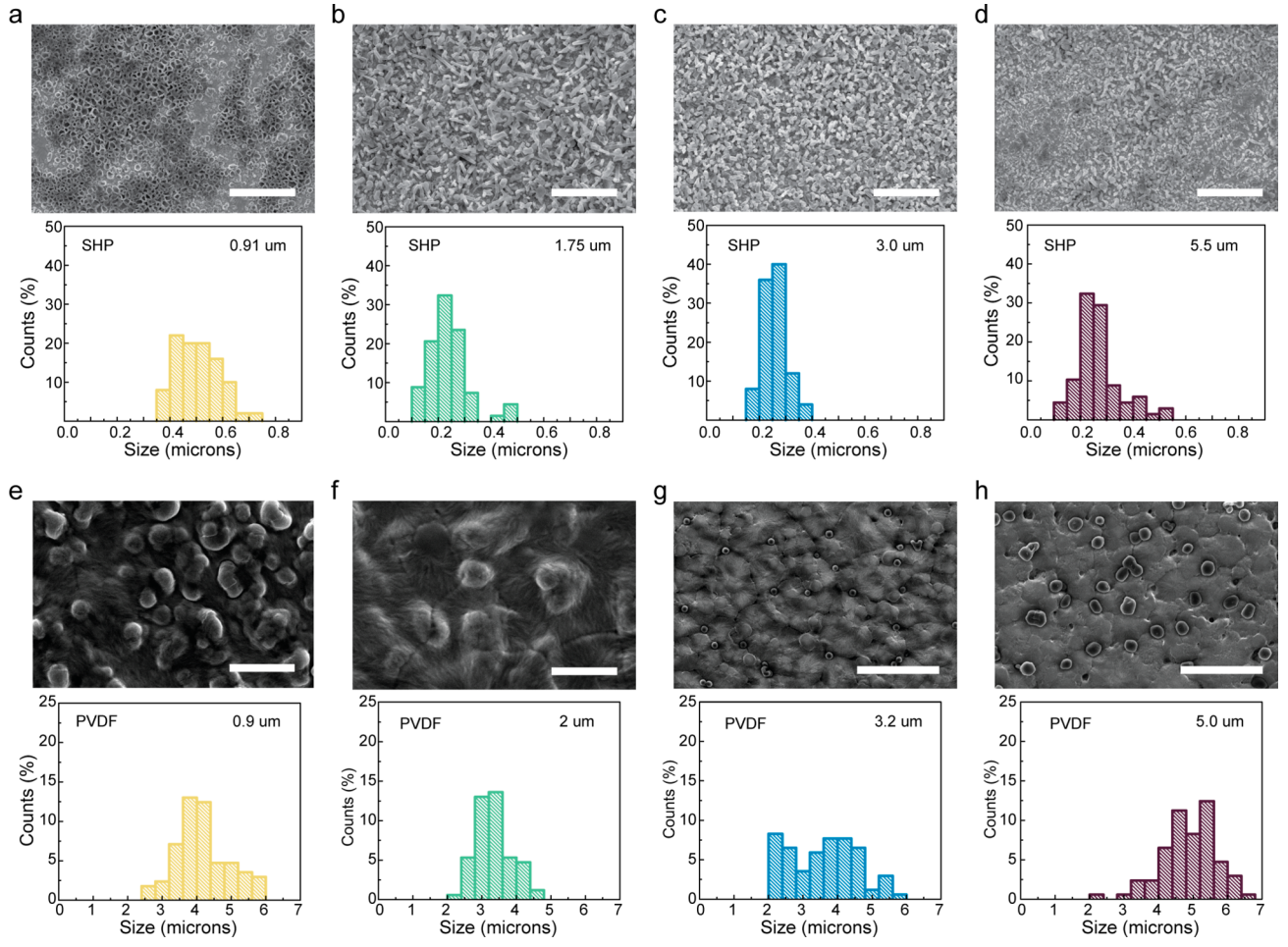

Figure 2. (a–d) SEM images of 0.1 mAh/cm^2 of lithium electrodeposited on copper with a SHP coating of variable thickness and histograms of the particle size for the SEM images. (e–g) SEM images of 0.1 mAh/cm^2 of lithium electrodeposited on copper with a PVDF coating of variable thickness and histograms of the particle size for the SEM images. Scale bars are 5 μm for images (a–f) and 30 μm for images (g and h).

and allow for the confident determination of the importance of these factors.

Coating Thickness. We began by examining the Li growth morphologies at the initial stages of deposition because these stages provide important indicators for final growth and represent the onset of interactions between Li metal and the electrolyte, SEI, and coatings.[35] We coated a layer of each polymer on copper (Cu) current collectors by spin coating and deposited 0.1 mAh cm^{-2} of Li (~500 nm equivalent thickness bulk Li) at 1 mA cm^{-2} underneath the polymer coating in 1 M

DOI: 10.1021/jacs.8b06047
J. Am. Chem. Soc. 2018, 140, 11735–11744

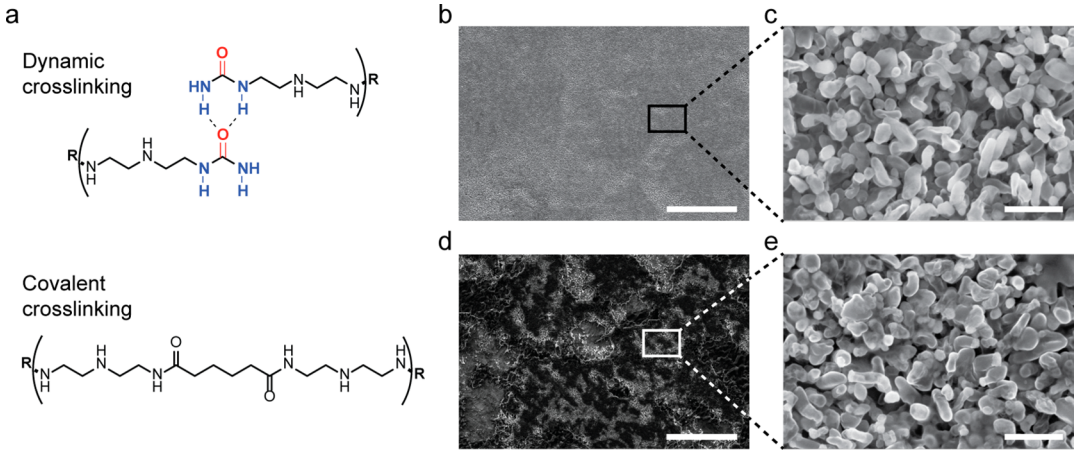

Figure 3. (a) Chemical structures of the dynamic cross-linking of the dynamic cross-linking of the SHP and covalent cross-linking of the SHE. SEM images of 0.1 mAh/cm^2 of lithium electrodeposited on polymer-coated copper. The electrodes are coated with (b, c) a supramolecular adaptive coating and (d, e) a covalently cross-linked self-healing elastomer with similar chemistry to the supramolecular coating. Scale bars are 50 μm for (b and d) and 1 μm for (c and e).

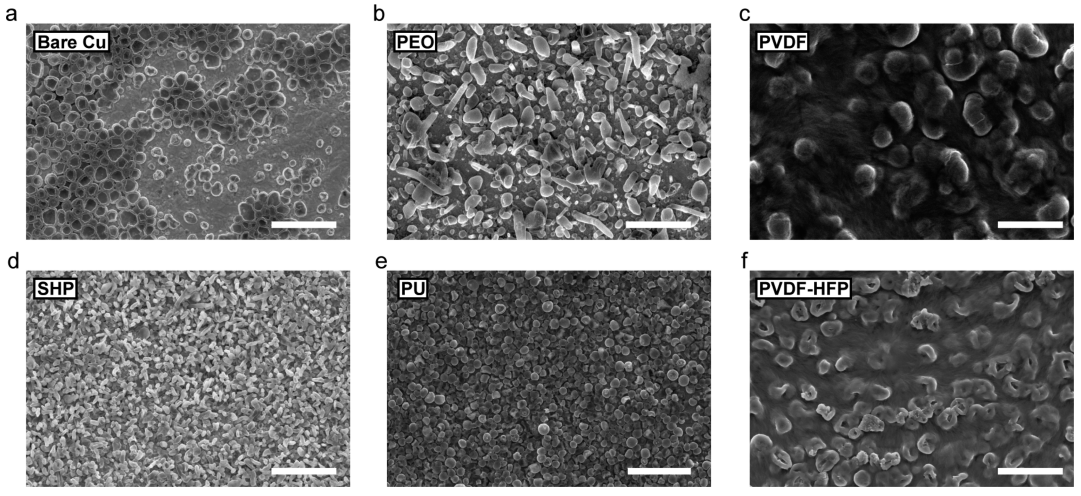

Figure 4. SEM images of 0.1 mAh/cm^2 of lithium electrodeposited on copper with (a) no polymer coating, (b) PEO coating, (c) PVDF coating, (d) SHP coating, (e) PU coating, and (f) PVDF-HFP coating. Scale bars for all images are 5 μm.

LiTFSI in 1:1(v/v) 1,3-dioxolane:1,2-dimethoxyethane (DOL:DME) with 1 wt % $LiNO_3$ as additive. We observed that the coating thickness significantly affected the uniformity and domain size of the Li deposits. The coating thickness was varied by modifying the solution concentration and spin coating parameters (Table S2). When SHP was coated with a thickness of 3 μm, the Li deposits formed uniform particles with a high density and uniformity across the electrode (Figure 2c). This uniformity was mostly maintained when the coating thickness was decreased to 1.75 μm (Figure 2b), but when the thickness was reduced to 0.91 μm, the deposits showed patchy growth and the characteristic round-shaped Li deposits of uncoated copper electrodes (Figure 2a), indicating that the coating was too thin to significantly influence spatial distribution of the Li nuclei. While the 0.91 μm SHP coating appeared to have no change in Li deposition compared to bare Cu, the particle size of ~500 nm was smaller than the 900 nm particle size measured for bare Cu (Figure S5). This indicates that the thin SHP coating still affects the nucleation processes but does not provide sufficiently uniform coating to influence the global deposit coverage. When the thickness is increased to 5.5 μm, the shape and size of the Li is unchanged, but the overall uniformity of the particle size and coverage is reduced (Figure 2d). Thicker coatings could decrease the uniformity of deposition due to ion transport limitations, as Li^+ ions are depleted from certain regions of the coating.

These qualitative observations are confirmed by statistical analysis of the SEM images. The 3 μm-thick films have the highest uniformity in particle size, with an average diameter of around 250 nm. Both the 1.75 and 5.5 μm films also grew particles with an average diameter of 250 nm, but their particle size distributions were broadened and slightly skewed toward larger Li deposits, reflecting the non-uniformity seen in the SEM. We observe similar effects when the thickness of the PVDF coating is varied. However, here we note that the optimal thickness is much thinner, 0.9 μm (Figure 2e). This is likely due to the lower ionic conductivity of the PVDF coating compared to the SHP coating (Table S1). A thicker covering of the PVDF is clearly observed over the Li particles for the 2 μm thick coating (Figure 2f), and for the 3.2 and 5 μm coatings, the Li begins to deposit via a different mechanism. For these two coatings there are larger deposits under the polymer coating, while smaller deposits grow through the pinholes in the film (Figure 2g,h). This indicates that PVDF

DOI: 10.1021/jacs.8b06047
J. Am. Chem. Soc. 2018, 140, 11735−11744

coatings thicker than ~2−3 μm are too thick to allow for uniform deposition and instead have two distinct deposition regimes, both under the polymer and through coating defects. Initially, Li metal nucleation begins at the polymer-copper interface, but as the Li particles grow in size they begin to grow through the defects in the polymer where ion transport is faster. Statistical analysis shows similar sizes and distributions for the coatings of 2 μm and below with an average diameter around 3.5 μm. For the coatings of 3 μm and above, the distribution is much broader due to the two different sizes of particles that are being grown. Overall, coatings that are too thin do not produce significant effects on the lithium deposition, and coatings that are too thick appear to hinder deposition. This indicates that coating thickness should be carefully optimized for future work in this field.

Coating Chemistry and Li Morphology. We compared the SHP and SHE coatings to understand the effects of polymer coating mechanics on Li deposition. Both polymers have similar chemistry, but the SHP is a flowable viscoelastic material, while the SHE is a covalently cross-linked elastic solid (Figures S1−S3). The high density of hydrogen bonding groups in the SHE still allows for self-healing to occur.[36] We observed that the overall uniformity of the Li deposition was very poor for the SHE compared to the flowable SHP (Figure 3b,d), indicating that the mechanical properties and coating quality of a polymer film are important for uniform deposition. However, when closely examining the individual Li deposits, we noticed that both the SHP and SHE coatings grew Li with nearly identical shapes (Figure 3c,e). This suggests that the chemical functionality of the polymer is a main factor dictating the local Li morphology.

To further investigate the effects of the chemistry of the polymer coating, we tested the other polymers described above. Every polymer coating tested was found to improve the coverage of initial Li deposits on the electrode over that of uncoated Cu, which showed many exposed regions of bare surface (Figure 4a). This suggests that the polymer coatings increased the density of lithium nucleation, leading to more uniform electrode coverage. However, this increased density of Li particles is not correlated to increases in the overpotential measured for the deposition as one would expect from classical nucleation theory (Table S1).[35] Interestingly, we also noticed that the shape or size of the Li particles changed depending on the polymer coating. For example, SHP and PEO altered the Li deposits to be very small in diameter (100s of nm) and nearly filamentary or rod-like in shape (Figure 4b,d), while PVDF and PVDF-HFP changed the Li particles to be much larger (1000s of nm) and globular (Figure 4c,f). Since there is no clear correlation of the Li deposit behavior with the modulus or viscoelasticity, it suggests that the polymer mechanical properties do not solely dictate Li morphology and cannot fully predict the intricate chemistry of lithium growth dynamics. This is especially clear when comparing the PEO and PVDF polymer coatings. Even though these materials have similar modulus and stress−strain behavior, the size and shape of the Li deposits differed drastically. It is possible that in situ changes to the mechanics of the polymer coatings due to swelling, interaction with dissolved ionic species, or reaction with the Li metal surface could account for this discrepancy, but these changes are difficult to measure and have thus been excluded from the present study.

Ultimately, particle size depends on both the nucleation and growth processes of the Li metal, which are influenced by the specific coating chemistry and will be discussed in later sections. Ideally, lithium metal would be deposited as a dense, uniform film on the electrode to minimize the contact area with the electrolyte and the potential for forming dead lithium particles electronically separated from the electrode. Coatings that promote this type of growth and are electrochemically stable over long-term battery cycling should provide the best performance.

Exchange Current Density. Initially, we presumed that the difference in nuclei size was a result of changes in the nucleation overpotential, as per classical nucleation theory.[35] However, we found that the differences in the overpotential for the Li nucleation event measured from the galvanostatic charging were not enough to explain the variation in nuclei size, let alone their shape or morphology (Table S1). This galvanostatic nucleation overpotential is a combination of all of the different overpotential components present in the coin cell including competition between the double layer capacitance and the nuclei growth.[37] In order to more accurately characterize the electrochemical processes occurring in the system, we turned to measuring the Li exchange current density which reflects the direct interaction of the polymer coating with the Li metal surface and can provide more precise information about the overpotential in the system. Generally, lower values of the exchange current density mean that the surface of the Li metal is inhibited or passivated, and in the field of electrodeposition, inhibition represents the degree to which additive molecules absorb to the active metal surface and suppress the reduction reaction. In the case of our control system (ether electrolyte with 1 wt % $LiNO_3$), the $LiNO_3$ acts as an inhibitor, which promotes the growth of rounded Li particles and improves the Coulombic efficiency.[38] For Li deposition on polymer-coated electrodes, the specific polymer coatings take on the role of inhibitors because they are directly in contact with the Li surface at the onset of and throughout deposition. Thus, the exchange current densities measured would ideally represent the level of inhibition or the strength of absorption and interaction of the polymers with the as-deposited Li metal and provide some relation to the Li morphology observed.

It is challenging to accurately measure the exchange current density in traditional coin cell geometries because of SEI forming reactions that occur on the surface of the Li metal. Fast sweep rates would allow this limitation to be overcome, but are generally not possible due to mass transport limitations. Here we utilized a home-built microelectrode, a technique known to overcome the mass transport limitations, to perform cyclic voltammetry sweeps at high rates of 200 mV/s. At these high sweep rates the freshly deposited Li is in direct contact with the polymer coating because the short time scale (~2 s) of the scan minimizes any reactions of the Li metal and electrolyte that may occur. These quick scan rates prevent resistive SEI formation from influencing the experiment and provide accurate measurement of the exchange current density, which reflects how the polymer coating interacts with the Li metal surface.

Electrochemical impedance spectroscopy (EIS) is sometimes used to measure the charge-transfer resistance and exchange current, but we have previously found that the charge-transfer resistances measured from Li|Li symmetric coin cells and by microelectrode could differ by orders of magnitude (0.1 mA/cm^2 vs 10s of mA/cm^2).[38] This discrepancy is because the high-frequency AC used in EIS

DOI: 10.1021/jacs.8b06047
J. Am. Chem. Soc. 2018, 140, 11735−11744

Table 2. Surface and Electrical Properties of Polymers Used in This Study

polymer	γ^a (mJ/m^2)	κ^b	$j_0{}^c$ (mA/cm^2)	CE^d (%)
DOL/DME	–	–	27	98.80 (±0.69)
PDMS	14.6 (±0.95)	2.77 (±0.30)	5 (±2.0)	99.42 (±0.05)
PEO	43.7 (±0.47)	5.42 (±0.35)	22 (±3.4)	98.71 (±0.05)
PU	40.8 (±2.5)	6.56 (±0.52)	20 (±5.5)	98.51 (±0.18)
PVDF	34.8 (±1.4)	10.0 (±1.75)	27 (±6.32)	99.11 (±0.15)
PVDF-HFP	31.0 (±1.5)	15.2 (±0.31)	39 (±10.6)	98.98 (±0.62)
SHP	38.6 (±0.43)	8.76 (±1.24)	27 (±5.4)	97.93 (±0.05)

[a]Surface energy. [b]Dielectric constant at 100 Hz. [c]Exchange current density. [d]Coulombic efficiency.

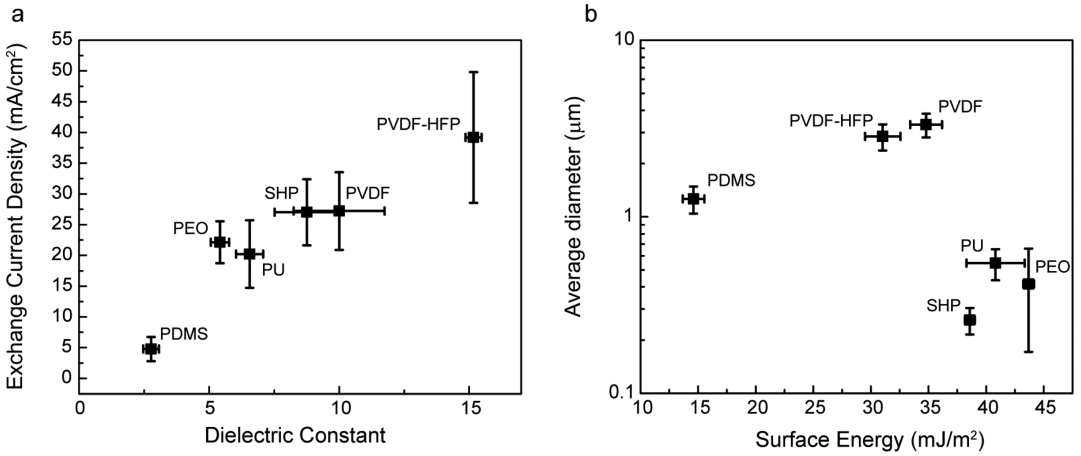

Figure 5. (a) Exchange current density plotted against dielectric constant for various polymer coatings measured via microelectrode. (b) The average diameter of the Li deposited under various polymer coatings plotted against the surface energy of those coatings. Error bars represent the standard deviation for all samples measured.

does not cause significant amounts of Li deposition. Thus, the kinetics probed by EIS here are mostly of Li^+ transported within the SEI, which is known to be a limiting factor.[39] So without fresh exposed Li from deposition, the charge-transfer resistance measured from a coin cell will be high. The microelectrode allows us to probe the properties of the Li surface that is directly in contact with the polymer coating and to minimize any effects that the SEI has on Li kinetics that would be present in normal EIS measurements.

Tafel plots are created from the high-rate CV scans (Figure S6) and the exchange current density (j_0) is extracted from the cathodic slope. Typical exchange current densities for Li in liquid electrolytes are 27 mA cm^{-2} for DOL/DME with 1 M LiTFSI and $LiNO_3$ (Table 2) and 35 mA cm^{-2} for EC/DEC with 1 M $LiPF_6$.[38] The polymer coatings tested here show exchange currents both lower and higher than these values, indicating that the materials we have selected cover a broad range of properties. PEO and PU both exhibit a low j_0 around 20 mA cm^{-2} and similarly contain ether groups throughout their backbones which may coordinate strongly with Li^+. In comparison, the SHP coatings show a higher j_0 of 26.9 mA cm^{-2} and have a combination of polar hydrogen bonding end groups and non polar, branched cores. The chemically similar fluorinated PVDF and PVDF-HFP both show higher j_0's of 27.2 mA cm^{-2} and 39.1 mA cm^{-2} respetively. Consistent with literature, we find that PDMS promotes the growth of moderate-sized Li particles (Figure S7),[25,27] and when examining the exchange current, we measured a very low j_0 of 4.7 mA cm^{-2}.

DISCUSSION

Exchange Current, Surface Energy, and Li Particle Size. As mentioned above, the mechanical properties of the polymer coating and the overpotential measured from galvanostatic deposition could not accurately predict the size of the Li particles that were deposited. We also found that the swelling, ionic conductivity, or resistance of the film did not follow any discernible trend (Table S1). However, we observed that the exchange current increased with dielectric constant of the polymer coating (Table 2 and Figure 5a). PVDF-HFP contains a high density of polarizable fluorinated groups and has a higher dielectric constant of 15. PVDF-HFP also exhibited the highest measured exchange current. PDMS has a much lower dielectric constant of 2.7 because of the nonpolar nature of the siloxane chemistry and exhibited the lowest exchange current measured. The other polymers tested have intermediate dielectric constants, and their exchange current densities fell in between that of PVDF-HFP and PDMS. We hypothesize that the relationship between dielectric constant and exchange current is due to the better solvation of Li^+ ions at the lithium-polymer interface from improved charge screening by the high dielectric constant coatings. This allows for easier dissolution and solvation of the Li from the metal electrode surface and could also increase the concentration of Li^+ ions available for deposition locally. These phenomena would cause an increase in exchange current between the Li metal surface and the electrolyte and are different effects from the adsorption-based inhibition that happens in the case of low-concentration additives added to electrolyte solutions.

We also noticed that in general, the size of Li deposits increased for the polymer coatings with higher exchange

DOI: 10.1021/jacs.8b06047
J. Am. Chem. Soc. 2018, 140, 11735−11744

current. However, PDMS presents a notable exception. Even though it has a very low exchange current due to a low dielectric constant, the Li deposited under the PDMS coating grows into large particles around 1.26 μm in size. When we re-examined the relationship between deposit size and other polymer properties, we found that PU, PEO, and SHP coatings all had high surface energy and promoted the growth of small Li particles around 100−400 nm in size (Figure 5b). The higher surface energy coatings should have enhanced adhesion to the Li metal surface compared to the lower surface energy polymers, and this stronger polymer-Li interaction serves to stabilize the Li-polymer interface. When both surface energy and exchange current are considered as relevant parameters, the anomalous size of the Li in the presence of the PDMS coating can be understood. The low surface energy of PDMS (14.6 mJ m^{-2}) resulted in a larger average particle size than the other polymers with low dielectric constants, but smaller than the ~3 μm particles from intermediate surface energy, high dielectric constant PVDF and PVDF-HFP.

This combined dependence of the Li particle size on both surface energy and exchange current becomes clear when the energetics of the nucleation process are analyzed.[35,40−42] A critical radius (r_{crit}) for Li nucleation can be found by examining the free energy for nucleating a new particle (ΔG_{nuc}). This free energy is the combination of the free energy for the bulk species (ΔG_{bulk}) and the energy required to create the new Li surface (ΔG_{surf}):[35,40−42]

$$\Delta G_{nuc} = \Delta G_{bulk} + \Delta G_{surf} \tag{1}$$

$$\Delta G_{nuc} = -\frac{zF|\eta|}{V_{molar}}V + \Gamma \times SA \tag{2}$$

where z is the number of electrons transferred, F is Faraday's constant, η is the overpotential, V_{molar} is the molar volume of lithium, Γ is the interfacial energy of the lithium metal surface, V is the volume of the nuclei, and SA is the surface area of the nuclei. The maximum in this function with respect to size of the new particles represents the transition from small unstable clusters to stable larger nuclei. Assuming that the nuclei are spherical and differentiating with respect to the radius of the nuclei yields the following as the critical radius size:[35,40]

$$r_{critical} = \frac{2\Gamma V_{molar}}{zF|\eta|} \tag{3}$$

From eq 3 one can see that changes in both Γ and η can affect the critical size of the nuclei. Γ can be defined in terms of the surface energies of the two materials in contact.[43] It is expressed as the following:

$$\Gamma = \gamma_{Li} + \gamma_{poly} - 2\Phi(\gamma_{Li}\gamma_{poly})^{1/2} \tag{4}$$

where γ_{Li} is the surface energy of the lithium metal, γ_{poly} is the surface energy of the polymer coating, and Φ is an interaction parameter for the two species. By expanding eq 4 with a Taylor series around the center of the surface energy data collected here (γ_{poly} = 30 mJ m^{-2}), we find that the second-order and higher terms are 2 orders of magnitude smaller than the linear term and that the first-order term is negative (Supporting Information). Therefore

$$\Gamma \propto -\gamma_{poly} \tag{5}$$

The Bulter−Volmer equation describes how the exchange current relates to the overpotential.[44] At high overpotential it reduces to the Tafel equation shown below for the case of a cathodic process:

$$-\eta = -A \ln\left(\frac{j}{j_0}\right) \tag{6}$$

$$-\eta \propto -\ln\left(\frac{j}{j_0}\right) \tag{7}$$

where A is known as the Tafel slope and j is the current density. From these two evaluations we can see that the nuclei size scales with both the surface energy of the polymer and the exchange current:

$$r_{crit} \propto \frac{-\gamma_{poly}}{\left|\ln\left(\frac{j}{j_0}\right)\right|} \tag{8}$$

As surface energy increases, the particle size decreases. Furthermore, as exchange current increases, the ratio of j/j_0 decreases which causes the overpotential to decrease. This decrease in overpotential causes an increase in the size of the nucleating Li particles.

In addition to the scaling described above, high dielectric constants and corresponding high exchanges currents serve to decrease the Li nucleation rate through decreased overpotential (eq 9) and increase the size of nucleation exclusion zones, resulting in more sparsely packed, larger Li deposits.[42] The nucleation rate (J) can be written as

$$J = K_1 \exp\left(-\frac{K_2}{\eta^2}\right) \tag{9}$$

where and K_1 and K_2 are constants that are practically independent of the overpotential.[40,42] Nucleation exclusion zones refer to the local deformations in the electric field that occur near the newly formed Li nuclei and cause an ohmic drop in the potential around the new nuclei. This potential drop prevents new nuclei from forming and is related to the exchange current. At high exchange current densities, the screening of the nuclei is poor, and so the exclusion zones are large leading to the growth of only the initial nuclei and thus larger particles. It should be noted, however, that these effects still enable relatively dense Li deposits without compromising the Li coverage of the electrode (Figure 4c,f).

Simultaneously, polymers with low surface energies have a weaker interaction with the Li metal and therefore do not reduce the polymer-Li interfacial energy as much as high surface energy polymers. With increased interfacial energy, the Li will deposit as larger particles to minimize surface area and reduce the total energy of the Li-polymer interface. This phenomena was suggested by Archer et al. in their calculations for polymer systems with immobilized anions.[33] Intuitively, both the chemical and ionic properties of the interface between the polymer coating and the Li metal surface should influence the Li deposition and growth. There should be interplay between the effects of polymer surface energy and exchange current; the swollen polymer coating at the Li interface serves critical roles in the deposition process as both a surface inhibitor and also as a localized electrolyte, mediating both charge-transfer and ionic transport. It may be the case that there is some cooperative inhibition behavior between the $LiNO_3$ and the polymer coatings, as has been observed in

DOI: 10.1021/jacs.8b06047
J. Am. Chem. Soc. 2018, 140, 11735−11744

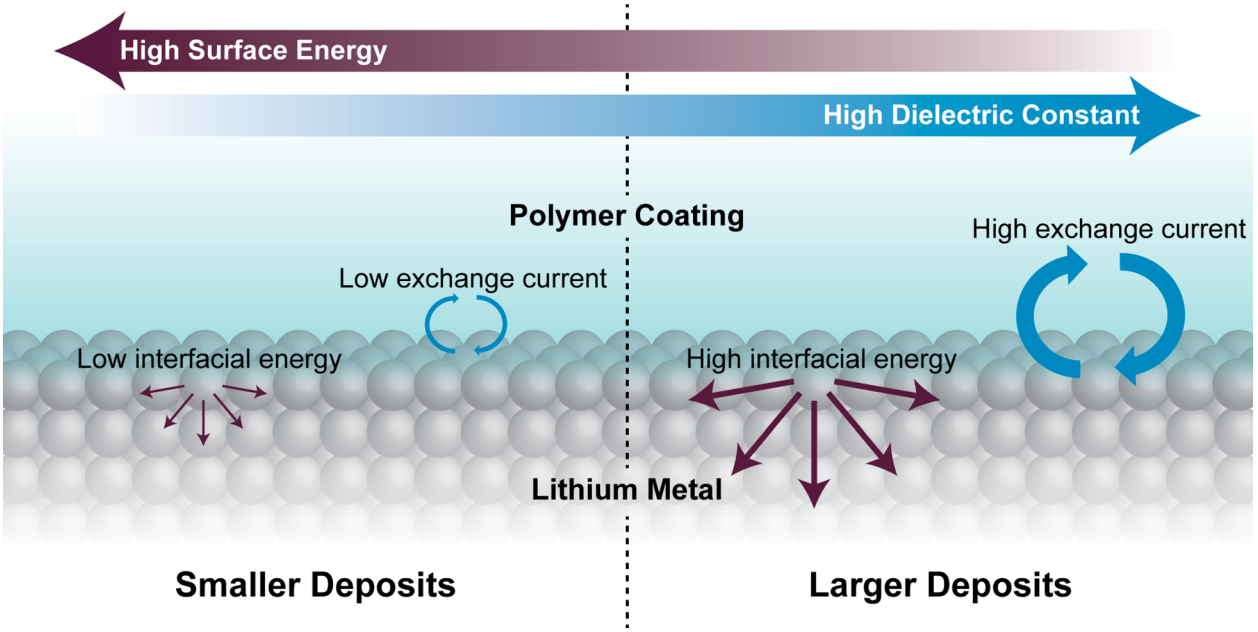

Figure 6. Schematic of the factors influencing Li metal deposition through a polymer coating. Low surface energy coatings give rise to higher interfacial energies and encourage the growth of large surface area particles. Additionally, high dielectric constant polymers have higher exchange currents and promote larger Li metal deposits.

traditional electrodeposition systems.[45] Further study of these cooperative effects should be pursued using the framework presented here. Figure 6 schematically illustrates the effects of the exchange current and interfacial energy on the Li particle size as described through the polymer dielectric constant and surface energy. In general, larger Li particles deposited under polymer coatings correspond to polymers with high dielectric constant and low surface energy.

Cycling Efficiency. Finally, we tested the Coulombic efficiency (CE) of the polymer coatings, as this is one of the most important factors for Li metal electrode performance. An average CE was measured by depositing a fixed reservoir of Li, cycling a fixed 1 mAh cm^{-2} capacity for 10 cycles, and then stripping all of the remaining Li.[46] Most of the coatings exhibited CEs around 98%, which is similar to the control case of the ether-based electrolyte. Notably, the PDMS coatings achieved a higher CE of 99.13%. There was no clear relationship between exchange current density and cycling CE. However, when we order the polymers by decreasing reactivity, an upward trend in the CE is observed (Figure 7). The reactivity of the different polymer coatings was estimated from their relative bond strengths. This is consistent with the present understanding that sub-100% efficiency of Li metal deposition/stripping is considered to be the result of parasitic side reactions and highlights the importance of polymer reactivity as an additional parameter. We also find that while CE is generally higher for polymer coatings that promote larger sized Li deposits (PVDF-HFP, PVDF, and PDMS), lower surface energy appears to be the best parameter that was recorded in this study for predicting high cycling CE.

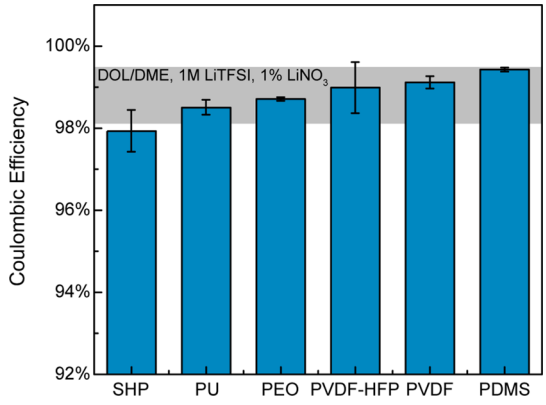

Figure 7. Coulombic efficiency of various polymer coatings. The horizontal axis is ordered in decreasing volume density of reactive groups. The gray bar represents the Coulombic efficiency of bare copper electrodes in DOL/DME electrolyte with 1 M LiTFSI and 1% $LiNO_3$.

CONCLUSION

In summary, by examining the initial stages of Li deposition and growth in the presence of polymer coatings, we have found that the chemistry of a polymer coating has significant impact on Li electrodeposition. The chemical functionality of a polymer coating resulted in different local Li deposit morphology, but coating mechanical properties, including modulus and flowability, and uniformity are still very important for the global deposition quality. We additionally found that the dielectric constant, and thus the solvation environment of the Li^+ ions, of the respective coatings determines the exchange current in the presence of polymer coatings. Furthermore, the size of the Li particles is dependent on both the dielectric constant, due to effects of the exchange current on nucleation, and surface energy, due to energetics of the Li-polymer interface, of the polymer coatings. Finally, both coating thickness and reactivity should additionally be considered as they both have large effects on coating performance. Moving forward, new coatings should be designed with high dielectric constant, low surface energy, and low reactivity. Ideally, a coating would also be soluble in nonpolar solvent or amenable to melt processing below lithium's T_m at 180 °C. This would allow for direct coating

DOI: 10.1021/jacs.8b06047
J. Am. Chem. Soc. 2018, 140, 11735−11744

on the Li metal surface, which is important for the fabrication of practical lithium metal batteries that are unlikely to be anodeless. The insight provided here should serve as a starting point for further systematic investigation into soft organic coatings that can potentially help to enable the uniform and reversible deposition of lithium metal at high rates and over long times.

■ ASSOCIATED CONTENT

Supporting Information

The Supporting Information is available free of charge on the ACS Publications website at DOI: 10.1021/jacs.8b06047.

Detailed description of the materials and methods, additional polymer characterization data, spin coating conditions, electrochemical characterization, and SEM. Additional discussion and details are provided for the Tafel slope fitting, interfacial energy scaling, coating reactivity, and surface energy calculations (PDF)

■ AUTHOR INFORMATION

Corresponding Authors

*zbao@stanford.edu

*yicui@stanford.edu

ORCID

Jeffrey Lopez: 0000-0002-6425-5550

Allen Pei: 0000-0001-8930-2125

Jin Young Oh: 0000-0003-2260-9960

Ging-Ji Nathan Wang: 0000-0002-5432-3046

Yi Cui: 0000-0002-6103-6352

Zhenan Bao: 0000-0002-0972-1715

Author Contributions

#These authors contributed equally.

Notes

The authors declare no competing financial interest.

■ ACKNOWLEDGMENTS

J.L. acknowledges support by the National Science Foundation Graduate Research Fellowship Program under grant no. (DGE-114747). A.P. acknowledges support by the Stanford Graduate Fellowship. The work was supported by the Assistant Secretary for Energy Efficiency and Renewable Energy, Office of Vehicle Technologies of the U.S. Department of Energy under the Battery 500 Consortium program. Part of this work was supported by BASF through the California Research Alliance (CARA) program. Part of this work was performed at the Stanford Nano Shared Facilities (SNSF), supported by the National Science Foundation under award ECCS-1542152. J.L. thanks D. S. Bergsman for helpful discussion regarding the mathematical analysis.

■ REFERENCES

(1) Xu, W.; Wang, J.; Ding, F.; Chen, X.; Nasybulin, E.; Zhang, Y.; Zhang, J.-G. *Energy Environ. Sci.* **2014**, *7* (2), 513−537.

(2) Lin, D.; Liu, Y.; Cui, Y. *Nat. Nanotechnol.* **2017**, *12* (3), 194−206.

(3) Chu, S.; Cui, Y.; Liu, N. *Nat. Mater.* **2017**, *16* (1), 16−22.

(4) Bruce, P. G.; Freunberger, S. A.; Hardwick, L. J.; Tarascon, J.-M. *Nat. Mater.* **2012**, *11* (1), 19−29.

(5) Pang, Q.; Liang, X.; Kwok, C. Y.; Nazar, L. F. *Nat. Energy* **2016**, *1* (9), 16132.

(6) Aurbach, D.; McCloskey, B. D.; Nazar, L. F.; Bruce, P. G. *Nat. Energy* **2016**, *1*, 16128.

(7) Whittingham, M. S. *Proc. IEEE* **2012**, *100*, 1518.

(8) Grey, C. P.; Tarascon, J. M. *Nat. Mater.* **2017**, *16* (1), 45−56.

(9) Yang, C.; Fu, K.; Zhang, Y.; Hitz, E.; Hu, L. *Adv. Mater.* **2017**, *29* (36), 1701169.

(10) Cheng, X.-B.; Zhang, R.; Zhao, C.-Z.; Zhang, Q. *Chem. Rev.* **2017**, *117* (15), 10403−10473.

(11) Duan, H.; Yin, Y. X.; Shi, Y.; Wang, P. F.; Zhang, X. D.; Yang, C. P.; Shi, J. L.; Wen, R.; Guo, Y. G.; Wan, L. J. *J. Am. Chem. Soc.* **2018**, *140* (1), 82−85.

(12) Zeng, X. X.; Yin, Y. X.; Shi, Y.; Zhang, X. D.; Yao, H. R.; Wen, R.; Wu, X. W.; Guo, Y. G. *Chem.* **2018**, *4* (2), 298−307.

(13) Qian, J.; Henderson, W. A.; Xu, W.; Bhattacharya, P.; Engelhard, M.; Borodin, O.; Zhang, J.-G. *Nat. Commun.* **2015**, *6*, 6362.

(14) Yang, C.; Chen, J.; Qing, T.; Fan, X.; Sun, W.; von Cresce, A.; Ding, M. S.; Borodin, O.; Vatamanu, J.; Schroeder, M. A.; Eidson, N.; Wang, C.; Xu, K. *Joule* **2017**, *1* (1), 122−132.

(15) Lu, Y.; Tu, Z.; Archer, L. A. *Nat. Mater.* **2014**, *13* (10), 961−969.

(16) Zheng, J.; Engelhard, M. H.; Mei, D.; Jiao, S.; Polzin, B. J.; Zhang, J.-G.; Xu, W. *Nat. Energy* **2017**, *2* (3), 17012.

(17) Li, W.; Yao, H.; Yan, K.; Zheng, G.; Liang, Z.; Chiang, Y.-M.; Cui, Y. *Nat. Commun.* **2015**, *6*, 7436.

(18) Tung, S.-O.; Ho, S.; Yang, M.; Zhang, R.; Kotov, N. A. *Nat. Commun.* **2015**, *6*, 6152.

(19) Bouchet, R.; Maria, S.; Meziane, R.; Aboulaich, A.; Lienafa, L.; Bonnet, J.-P.; Phan, T. N. T.; Bertin, D.; Gigmes, D.; Devaux, D.; Denoyel, R.; Armand, M. *Nat. Mater.* **2013**, *12* (5), 452−457.

(20) Choudhury, S.; Mangal, R.; Agrawal, A.; Archer, L. A. *Nat. Commun.* **2015**, *6*, 10101.

(21) Khurana, R.; Schaefer, J. L.; Archer, L. A.; Coates, G. W. *J. Am. Chem. Soc.* **2014**, *136* (20), 7395−7402.

(22) Lu, Q.; He, Y.-B.; Yu, Q.; Li, B.; Kaneti, Y. V.; Yao, Y.; Kang, F.; Yang, Q.-H. *Adv. Mater.* **2017**, *29* (13), 1604460.

(23) Zheng, G.; Lee, S. W.; Liang, Z.; Lee, H.-W.; Yan, K.; Yao, H.; Wang, H.; Li, W.; Chu, S.; Cui, Y. *Nat. Nanotechnol.* **2014**, *9* (8), 618−623.

(24) Yan, K.; Lee, H.-W.; Gao, T.; Zheng, G.; Yao, H.; Wang, H.; Lu, Z.; Zhou, Y.; Liang, Z.; Liu, Z.; Chu, S.; Cui, Y. *Nano Lett.* **2014**, *14* (10), 6016−6022.

(25) Zhu, B.; Jin, Y.; Hu, X.; Zheng, Q.; Zhang, S.; Wang, Q.; Zhu, J. *Adv. Mater.* **2017**, *29* (2), 1603755.

(26) Zheng, G.; Wang, C.; Pei, A.; Lopez, J.; Shi, F.; Chen, Z.; Sendek, A. D.; Lee, H.-W.; Lu, Z.; Schneider, H.; Safont-Sempere, M. M.; Chu, S.; Bao, Z.; Cui, Y. *ACS Energy Lett.* **2016**, *1*, 1247−1255.

(27) Liu, K.; Pei, A.; Lee, H. R.; Kong, B.; Liu, N.; Lin, D.; Liu, Y.; Liu, C.; Hsu, P.-C.; Bao, Z.; Cui, Y. *J. Am. Chem. Soc.* **2017**, *139* (13), 4815−4820.

(28) Li, N.-W.; Shi, Y.; Yin, Y.-X.; Zeng, X.-X.; Li, J.-Y.; Li, C.-J.; Wan, L.-J.; Wen, R.; Guo, Y.-G. *Angew. Chem., Int. Ed.* **2018**, *57* (6), 1505−1509.

(29) Liu, Y.; Lin, D.; Yuen, P. Y.; Liu, K.; Xie, J.; Dauskardt, R. H.; Cui, Y. *Adv. Mater.* **2017**, *29* (10), 1605531.

(30) Song, J.; Lee, H.; Choo, M.-J.; Park, J.-K.; Kim, H.-T. *Sci. Rep.* **2015**, *5*, 14458.

(31) Luo, J.; Fang, C.-C.; Wu, N.-L. *Adv. Energy Mater.* **2018**, *8* (2), 1701482.

(32) Gao, Y.; Zhao, Y.; Li, Y. C.; Huang, Q.; Mallouk, T. E.; Wang, D. *J. Am. Chem. Soc.* **2017**, *139* (43), 15288−15291.

(33) Tikekar, M. D.; Archer, L. A.; Koch, D. L. *Science Advances* **2016**, *2* (7), e1600320−e1600320.

(34) Monroe, C.; Newman, J. *J. Electrochem. Soc.* **2005**, *152* (2), A396.

(35) Pei, A.; Zheng, G.; Shi, F.; Li, Y.; Cui, Y. *Nano Lett.* **2017**, *17* (2), 1132−1139.

(36) Sun, Y.; Lopez, J.; Lee, H.-W.; Liu, N.; Zheng, G.; Wu, C.-L.; Sun, J.; Liu, W.; Chung, J. W.; Bao, Z.; Cui, Y. *Adv. Mater.* **2016**, *28* (12), 2455−2461.

(37) Lin, D.; Liu, Y.; Pei, A.; Cui, Y. *Nano Res.* **2017**, *10* (12), 4003−4026.
(38) Shi, F.; Pei, A.; Vailionis, A.; Xie, J.; Liu, B.; Zhao, J.; Gong, Y.; Cui, Y. *Proc. Natl. Acad. Sci. U. S. A.* **2017**, *114* (46), 12138−12143.
(39) Shi, F.; Pei, A.; Boyle, D. T.; Xie, J.; Yu, X.; Zhang, X.; Cui, Y. *Proc. Natl. Acad. Sci. U. S. A.* **2018**, *115*, 8529.
(40) Plieth, W. *Electrochemistry for Materials Science*; Elsevier: Amsterdam, 2008.
(41) Sagane, F.; Ikeda, K.; Okita, K.; Sano, H.; Sakaebe, H.; Iriyama, Y. *J. Power Sources* **2013**, *233*, 34−42.
(42) Popov, K. I.; Djokić, S. S.; Nikolić, N. D.; Jović, V. D. *Morphology of Electrochemically and Chemically Deposited Metals*; Springer International Publishing: Switzerland, 2016.
(43) Girifalco, L. A.; Good, R. J. *J. Phys. Chem.* **1957**, *61* (7), 904−909.
(44) Bard, A. J.; Faulkner, L. R. *Electrochemical Methods: Fundamentals and Applications*, 2nd ed.; Wiley Global Education: New York, 2000.
(45) Kelly, J. K.; Tian, C.; West, A. C. *J. Electrochem. Soc.* **1999**, *146*, 2540−2545.
(46) Adams, B. D.; Zheng, J.; Ren, X.; Xu, W.; Zhang, J.-G. *Adv. Energy Mater.* **2018**, *8*, 1702097.

DOI: 10.1021/jacs.8b06047
J. Am. Chem. Soc. 2018, 140, 11735−11744